Journal of Materials Chemistry A

Accepted Manuscript

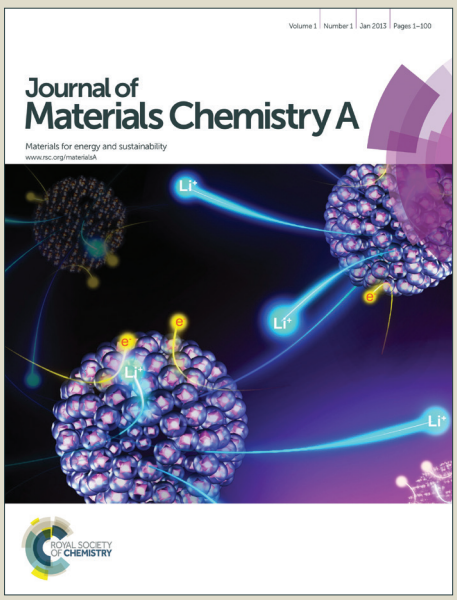

ROYAL SOCIETY OF CHEMISTRY

www.rsc.org/materialsA

Graphics abstract

Newly-designed sandwich-structured graphene-Pt-graphene catalyst with improved electrocatalytic performance for fuel cells

Lei Zhao,[a] Zhen-Bo Wang,*[a] Jia-Long Li,[a] Jing-Jia Zhang,[a] Xu-Lei Sui,[a] Li-Mei Zhang[a]

[a] School of Chemical Engineering and Technology, Harbin Institute of Technology, No.92 West-Da Zhi Street, Harbin, 150001 China

* Corresponding author. Tel.: +86-451-86417853; Fax: +86-451-86418616

E-mail address: wangzhb@hit.edu.cn

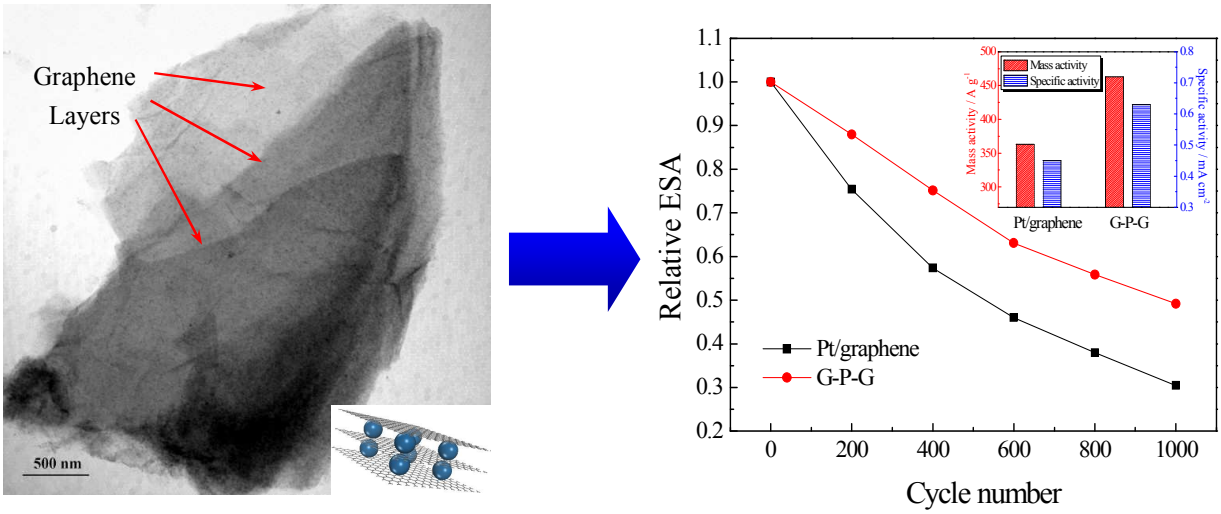

A Novel Sandwich-structured G-P-G catalyst prepared by a simple, facile synthesis method exhibits 1.27 times higher activity for methanol electro-oxidation than that of Pt/graphene and the stability is improved by 70% as compared with Pt/graphene.

ARTICLE TYPE
www.rsc.org/xxxxxx | XXXXXXXX

Newly-designed sandwich-structured graphene-Pt-graphene catalyst with improved electrocatalytic performance for fuel cells

Lei Zhao,[a] Zhen-Bo Wang,*[a] Jia-Long Li,[a] Jing-Jia Zhang,[a] Xu-Lei Sui,[a] Li-Mei Zhang[a]

Received (in XXX, XXX) Xth XXXXXXXXX 200X, Accepted Xth XXXXXXXXX 200X
First published on the web Xth XXXXXXXXX 200X
DOI: 10.1039/b000000x

A novel sandwich-structured graphene-Pt-graphene (G-P-G) catalyst has been synthesized by a convenient approach. The obtained G-P-G catalyst has been characterized by X-ray diffraction, X-Ray photoelectron spectroscopy, scanning electron microscopy, transmission electron microscopy, high resolution transmission electron microscopy, and electrochemical measurements. Structural characterization presents G-P-G catalyst with well-defined sandwich-like morphology. The results of electrochemical measurements indicate that the G-P-G exhibits 1.27 times higher activity for methanol electrooxidation than that of Pt/graphene catalyst. Importantly, the results of accelerated potential cycling test demonstrate that G-P-G catalyst possesses 1.7 times as high stability as that of Pt/graphene. The significantly enhanced electrochemical performance is ascribed to the unique sandwich-like structure. Pt nanoparticles are anchored between the two adjacent graphene sheets, substantially enhancing metal-support interaction, and graphene could act as a "mesh bag" to prevent the Pt species from leaking into the electrolyte, so its stability has considerably been enhanced. The effect of composited graphene amount in the hybrid has also been systematically studied. The stability of the catalyst increases with the increasing of introduced GO amount and the G-P-G_{50} show the optimized electrocatalytic performance. These findings suggest that sandwich-structured G-P-G catalyst holds tremendous promise for fuel cells.

1. Introduction

Although great progress has been made in the research and development of proton exchange membrane fuel cell (PEMFC) in terms of performance increases and cost reduction,[1-3] some obstacles, such as lifetime, reliability and cost, still exist and impede its commercialization.[4-6] So to move towards a genuinely practical technology that can be scale-manufactured cost-effectively, significant improvements are still needed.[7, 8] Various kinds of carbon materials are widely used as the support for fuel cell catalysts because of their high surface area, good electronic conductivity, and appropriate pore structure.[9-11] However, the corrosion of carbon support is unavoidable,[12] especially in the harsh operating environment of the fuel cells.[13, 14] It is reported that the extent of graphitization of the carbon plays an important role on the stability of carbon support, the higher the degree of graphitization, the better the stability.[15, 16] A large amount of attention is paid on novel carbon nanostructure materials,[17-19] e.g., carbon nanotubes (CNT),[20] carbon nanofibers (CNF),[21] mesoporous carbon (MC),[22] etc. for application as catalyst support.

Graphene,[23-25] as a two-dimensional (2D) sheet with fully delocalized π-electrons, quickly became the subject of intense research by physicists, chemists and material scientists since its discovery by Geim et al. in 2004.[26] Notable effort has been devoted to the design of novel nanocatalyst dispersed on graphene. Nevertheless, irreversible agglomeration caused by van der Waals force made Pt nanoparticles (NPs) difficult to distribute homogeneously on the surface of graphene.[27, 28] Actually, graphene supported Pt catalysts have been extensively investigated and employed as electrocatalysts for fuel cells.[29, 30] However, some serious problem such as stability and poisoning of Pt-based catalysts by CO-like intermediates would also limit their further applications as support for fuel cell catalyst. Recently, the combination of carbon/noncarbon materials with graphene as support is a popular way to enhance the performance of the catalyst.[31-33] Lou and his co-workers[34] have developed a facile strategy to prepare novel Pt-TiO_2-rGO 3-component electrocatalysts with significantly enhanced electrocatalytic performance for methanol electrooxidation. Mu and his co-workers[35] report a nano-sandwiched structured graphene/carbon nanosphere/graphene (GCG) composite prepared by a novel, simple method using low cost carbon nanosphere materials as pillars between the graphene layers. Moreover, Pt/GCG showed a much better stability and higher activity in electrochemical surface area and half cell oxygen reduction activity compared with the Pt/graphene and Pt/C catalysts. Nonetheless, the addition of carbon/noncarbon materials will increase the complexity of the synthesis process and carbon materials can be still electrochemically oxidized under the harsh work environment of PEMFC. Therefore, it is of great importance and necessary to develop a convenient and effective strategy for novel structured graphene supported Pt catalysts with high electrocatalytic activity and stability.

In this work, we present graphene-Pt-graphene (G-P-G) catalyst with well-defined nanosheet-like morphology and excellent electrocatalytic activity. G-P-G catalyst was prepared by a simple,

[a] *School of Chemical Engineering and Technology, Harbin Institute of Technology, No.92 West-Da Zhi Street, Harbin, 150001 China. E-mail: wangzhb@hit.edu.cn; Tel.: +86-451-86417853; Fax: +86-451-86418616*

† Electronic supplementary information (ESI) available. See DOI: 10.1039/b000000x

facile synthesis method. Graphene supported Pt catalyst was synthesized using a fast and facile microwave-assisted polyol process, then with the introduction graphene into the mixture, the sandwich-structured G-P-G catalyst can be obtained. The overall procedure does not require complicated steps. Pt NPs are anchored between the two adjacent graphene sheets, which is beneficial for improving the stability of the catalysts. Results of the electrochemical measurements show that these G-P-G catalysts exhibit significantly improved electrocatalytic performance due to the novel sandwich-like structure.

2. Experimental

2.1. Materials

Hexachloroplatinic acid ($H_2PtCl_6 \cdot 6H_2O$) was purchased from Shanghai, China. 5 wt.% Nafion solution was purchased from Dupont and Graphite was obtained from Alfa Aesar. Except where specified, all chemicals were of analytical grade and used as received.

2.2. Catalyst preparation

Graphite oxide (GO) was synthesized from graphite powder by modified Hummer's method.[36] Pt/graphene catalyst was synthesized by a microwave-assisted polyol process (MAPP). Briefly, a calculated amount of GO was dispersed into the mixture of ethylene glycol (EG) and isopropyl alcohol under ultrasonic treatment (from Shanghai, 53 KHz, 280 W) for 1 h. Then H_2PtCl_6-EG solution was added into the uniform ink with agitation for 3 h. The pH value of the ink was then adjusted to about 12.0 and the suspension was subjected to consecutive microwave heating for 64 s. After cooling to room temperature, the pH value of the solution was adjusted to 2-3. The mixture was kept stirring for 12 h and then the product was washed repeatedly with ultrapure water (Millipore, 18.2 MΩ·cm). The sandwich-structured G-P-G catalyst was synthesized by the same procedure for preparing the Pt/graphene, but before washing the catalyst, a calculated amount of GO was added into the mixture under ultrasonic treatment and followed by heating the solution under flowing argon at 140 ^oC for 1.5 h. Subsequently, the product was washed repeatedly with ultrapure water (18.2 MΩ·cm). The sandwich-structured graphene-Pt/TiO_2-graphene (G-Pt/TiO_2-G) catalyst was synthesized by the same procedures as for preparing the G-P-G catalyst, but the initial GO was replaced by the combination of GO with anatase TiO_2. The obtained Pt/graphene and G-P-G catalyst was dried for 5 h at 80 ^oC in a vacuum oven and then stored in a vacuum vessel.

2.3. Physical characterization

X-ray diffraction (XRD) analysis of as-prepared catalyst was carried out with the D/max-RB diffractometer (made in Japan) using a Cu Kα X-ray source operating at 45 kV and 100 mA, scanning at a rate of 4^o min^{-1} with an angular resolution of 0.05^o of the 2θ scan to get the XRD pattern. Field emission scanning electron microscope (SEM, Hitachi Ltd. S-4700) was used to characterize the morphologies and structures of the catalyst. The samples were supported on the aluminum foil to eliminate the influence of the conductive carbon tape. Transmission electron microscopy (TEM) and high resolution transmission electron microscopy (HRTEM) for the catalyst samples were taken by a TECNAI G2 F30 field emission transmission electron microscope. Before taking the electron micrographs, the samples were finely ground and ultrasonically dispersed in alcohol, and a drop of the resultant dispersion was deposited and dried on a standard copper grid coated with carbon film. The applied voltage was 300 kV. X-Ray photoelectron spectroscopy (XPS) analysis was carried out with a physical electronics PHI model 5700 instrument. The Al X-ray source was operated at 250 W and the take-off angle of the sample to analyzer was 45^o. Survey spectra were collected at pass energy (PE) of 187.85 eV over a binding energy range from 0 eV to 1300 eV. High binding energy resolution multiplex data for the individual elements were collected at a PE of 29.55 eV. During all XPS experiments, the pressure inside the vacuum system was maintained at 1×10^{-9} Pa. Before the analysis above, all the samples were dried under vacuum at 80^{o}C overnight. Raman spectra of simples were measured using a Renishaw1000 Raman microscope (Rhenishaw Instruments, England) using a 532 nm argon ion laser.

2.4 Electrochemical measurements

All electrochemical measurements were carried out in a standard three-electrode cell using a CHI 650E electrochemical analysis instrument at an ambient temperature, with a platinum wire as the counter electrode, Hg/Hg_2SO_4 (0.68 V relative to reversible hydrogen electrode, RHE) as the reference electrode, and a glassy carbon disk electrode as the working electrode. Working electrodes were prepared as follows: 2.0 mg catalyst in 2.0 mL ethanol was ultrasonicated for 20 min. Then, 10 μL of this ink was transferred onto a glassy carbon disk (GC, 4 mm diameter), and onto which 5 μL of a dilute aqueous Nafion® solution (5 wt. % solution in a mixture of lower aliphatic alcohols and ultrapure water) was added. The cyclic voltammograms (CV) measurements for evaluating methanol oxidation performance were recorded within a potential range from 0.05 V to 1.2 V (vs. RHE) at a scan rate of 50 mV/s in a Ar-saturated 0.5 M H_2SO_4 electrolyte containing 0.5 M CH_3OH.

To investigate the stability of catalysts, the accelerated potential cycling test (APCT) within the potential range of 0.6 to 1.2 V (vs. RHE) was applied. The electrochemical active specific surface areas (ESA)[37] of platinum with coulombic charges accumulated during hydrogen adsorption or desorption after correcting for the double-layer charging current from the CVs can be calculated:[38]

$$ESA = \frac{Q_H}{0.21 \times M_{Pt}} \quad (1)$$

Where Q_H (mC) is the charge due to the hydrogen adsorption/desorption in the hydrogen region of the CVs, 0.21 mC cm^{-2} is the electrical charge associated with monolayer adsorption of hydrogen on Pt metal, and M_{Pt} is the loading of Pt metal on the working electrode. The catalytic stability of methanol oxidation was performed by the chronoamperometric curves at a constant potential of 0.6 V vs. RHE for 3600 s in a solution of 0.5 mol L^{-1} H_2SO_4 containing 0.5 mol L^{-1} CH_3OH.

3. Results and discussion

Scheme 1 shows the principle steps of preparation process of sandwich-structured G-P-G hybrid catalysts as follows: Firstly, Pt NPs were deposited on the surface of graphene through a MAPP. Then with the introduction of graphene on the surface of Pt NPs,

the desired graphene-Pt-graphene (G-P-G) hybrid can be obtained. Interestingly, Pt NPs were designed to deposit between graphene layers. The G-P-G hybrid catalysts exhibit significantly enhanced electrochemical performance can be ascribed to the novel sandwich structure.

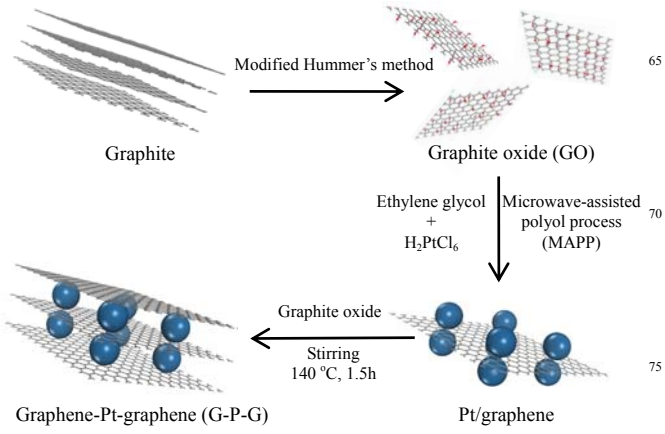

Scheme 1 Schematic illustration of the preparation of the sandwich-structured G-P-G hybrid catalyst.

The XRD patterns of GO, Pt/graphene and G-P-G hybrid catalyst are shown in Fig. 1. In Fig. 1a, the characteristic diffraction peak (002) of GO at around 11.4° is ascribed to the introduction of oxygenated functional groups on both sides and edges of carbon sheets. It indicates that GO has been successfully obtained via the chemical oxidation of graphite powder. Pt/graphene catalyst (Fig. 1b) possesses a broad diffraction peak at 24.1° corresponding to the (002) plane of graphene indicating that the GO has been reduced to graphene during the MAPP. The strong diffraction peaks at 2 θ = 39.7°, 67.2° and 81.6° can be assigned to the characteristic (111), (220) and (311) crystalline planes of Pt, respectively, which possesses face-centered-cubic (fcc) structure. The XRD pattern of G-P-G catalyst is similar to Pt/graphene, however, the diffraction peaks of Pt (220), (311) are not clear due to lower Pt content of G-P-G catalyst than Pt/graphene.

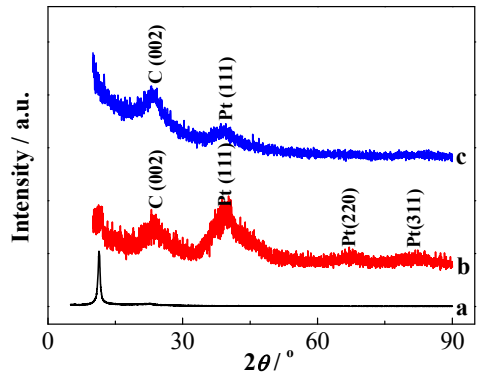

Fig. 1 XRD patterns of GO (a), Pt/graphene (b) and sandwich-structured G-P-G catalyst (c).

The composition of carbon atoms in the synthesized catalysts was analyzed by XPS. Fig. 2 presents the C1s XPS spectra of GO and G-P-G catalyst (for Pt/graphene, see Fig. S1). The binding energy of 284.5 eV is attributed to the C-C bonds, and the ones of 286.7 eV and 288.8 eV are typically assigned to the C-O and C=O functional groups, respectively. Here the C-O bonds include epoxide (-O-) and hydroxyl (-OH); C=O bonds include carbonyl (-C=O), carboxyl (-COOH), and carboxylate (-COOR).[39] The C1s peaks in the Pt/graphene and G-P-G catalyst exhibit the same oxygen functionalities as those that have been assigned to GO, while some peak intensities are much smaller than those in GO, indicating considerable deoxygenation of GO by the reduction process. In addition, XPS also presents the reduction of Pt NPs during the MAPP (Fig. S1).

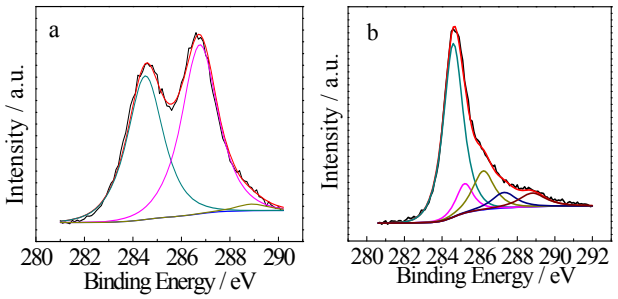

Fig. 2 XPS spectra of the C1s in GO (a) and G-P-G catalyst (b)

The structural changes of GO during the preparation of the G-P-G hybrid catalyst is reflected in their Raman spectra (Fig. S2). The Raman spectrum of G-P-G catalyst shows two peaks at ~1332 and ~1592 cm^{-1} corresponding to the D (breathing mode of A_{1g} symmetry) and G (E_{2g} symmetry of sp^2 carbon atoms) bands, respectively.[40] The intensity ratio of the D to G (I_D/I_G) in the case of GO is found to be 0.92, while in G-P-G hybrid catalyst is 1.03, suggesting a decrease of sp^2-domain induced by the reduction of GO through polyol process.

The typical SEM images of sandwich-structured G-P-G hybrid catalyst are shown in Fig. 3, which show the graphene sheet stack together (Fig. 3a and b) and Pt NPs deposit uniformly between graphene layers (Fig. 3c). TEM characterization of a typical G-P-G hybrid catalyst disclosed that graphene-Pt-graphene sandwich structure has been obtained (Fig. 3d and S3).

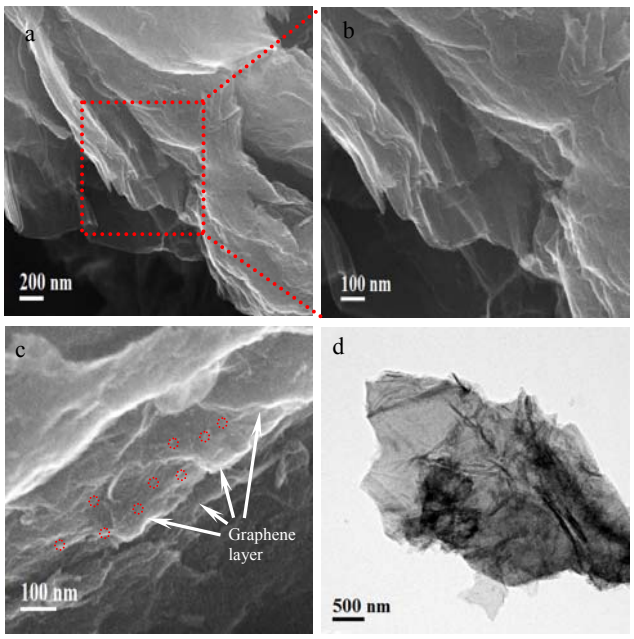

Fig. 3 SEM images (a,b,c) and TEM images (d) of G-P-G hybrid catalyst.

The sandwich-structured G-P-G hybrid catalysts are further confirmed by TEM techniques. Fig. 4a visibly reveals graphene and Pt NPs stack together orderly forming the unique layered stacking sandwich-structured G-P-G hybrid catalysts. It can be seen distinctly that morphology of G-P-G hybrid catalysts is entirely different from that of Pt/graphene (Fig. S4). TEM images of Pt/graphene show Pt NPs deposit on the almost transparent carbon sheets with a typically crumpled surface. By contrast, introducing graphene on the surface of Pt NPs, the obtained G-P-G hybrid catalysts (Fig. 4a) exhibit a novel 3D sandwich nanoarchitecture. It is further convinced that the sandwich-structured G-P-G hybrid catalysts are fabricated successfully by observing the edge of the catalyst (Fig. 4b). It can be observed from Fig. 4c that the G-P-G hybrid catalysts contain three layers of graphene, meanwhile, the uniform distribution of the Pt NPs can also be verified. It is supposed that the unique sandwich-like structures of the graphene-Pt-graphene will anchor the Pt NPs, and be beneficial for improving the stability of the catalysts. Since graphene is separated by Pt NPs with sizes of about 2 nm, the sandwich-structured hybrid catalysts will allow the reactants (methanol in here) to fully touch the Pt NPs, and provide enough space for mass transfer of reactant and products. HRTEM image of G-P-G hybrid catalysts was also measured and the typical results are shown in Fig. 4d. It can be seen clearly the regular lattice fringes with a spacing of 0.227 nm, which is highly consistent with the (111) plane of Pt.

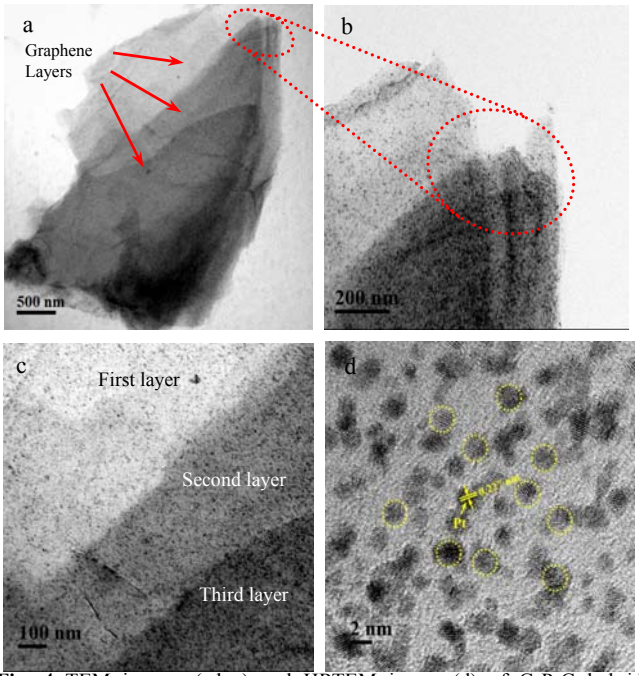

Fig. 4 TEM images (a,b,c) and HRTEM image (d) of G-P-G hybrid catalyst.

We compared the particle size of Pt in Pt/graphene and G-P-G hybrid catalysts in order to elucidate changes of Pt NPs during the preparation process for G-P-G hybrid catalysts. The changes of Pt NPs during APCT process are also investigated. Additional TEM images with associated size distributions before and after APCT are available in Fig. 5. TEM images show that the dispersion of Pt NPs in Pt/graphene and G-P-G hybrid catalysts is fairly uniform and the mean sizes of Pt NPs of the catalyst are estimated to be 2.13 and 2.16 nm. It can be observed that the mean size of Pt NPs in Pt/graphene catalyst is almost the same as that in G-P-G hybrid catalyst before APCT. It can be confirmed that the particle size of Pt is not affected by the sandwich structure and their difference of electrochemical performance is not caused by Pt nanoparticle size. However, after the APCT, the crystallite sizes of Pt/graphene, and G-P-G grow to 4.39 and 4.21nm, increasing by 106.1, and 94.9% in comparison with those before APCT, respectively. More important, the dispersion of Pt NPs in G-P-G is more uniform than that in Pt/graphene catalyst, suggesting G-P-G catalysts possess a better stability.

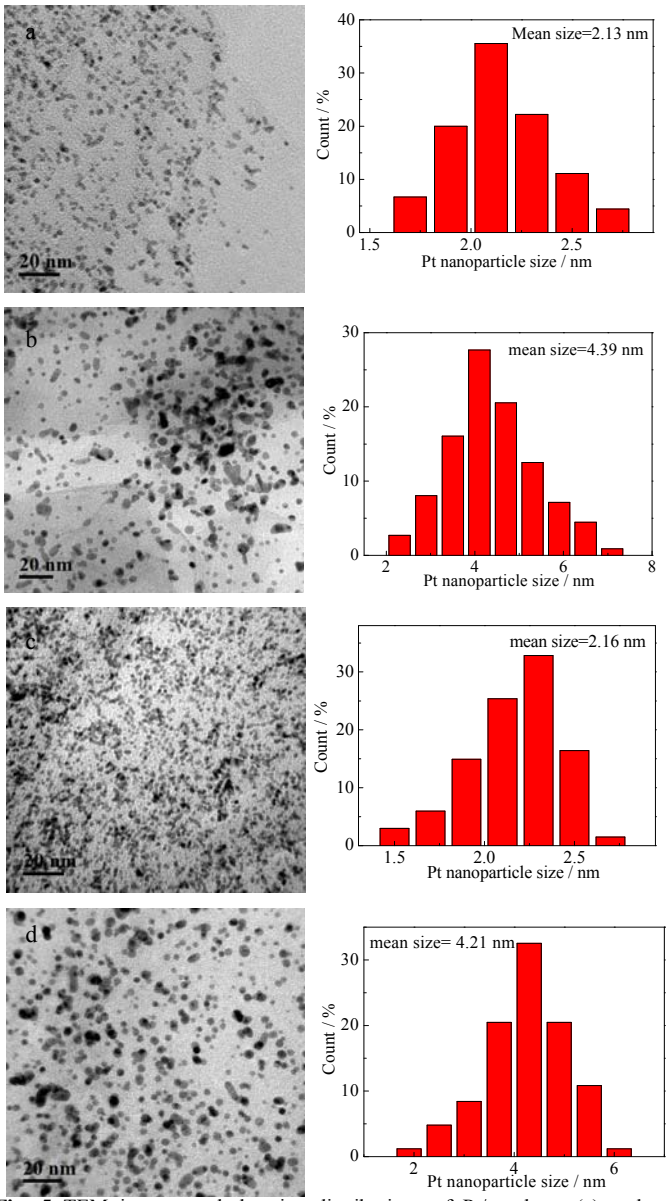

Fig. 5 TEM images and the size distributions of Pt/graphene (a) and sandwich structured G-P-G hybrid catalysts (b).

Fig. 6 depicts the CV curves for methanol electrooxidation reaction (MOR) on Pt/graphene and sandwich-structured G-P-G catalysts in an Ar-saturated solution of 0.5 mol L^{-1} H_2SO_4 containing 0.5 mol L^{-1} CH_3OH at 25 ^oC. The ESA of catalysts are calculated from CVs in a solution of 0.5 mol L^{-1} H_2SO_4 (Fig. S5). Their ESA are determined through the charge due to hydrogen

adsorption/desorption according to the equation (1). The ESA of Pt/graphene is 80.9 $m^2 g^{-1}$, which is a little higher than that of G-P-G catalysts (73.9 $m^2 \cdot g^{-1}$). It also proves that Pt particle active sites are indeed partly covered by the sandwich-like structure. However, the Pt NPs on the graphene surface act as nanoscale spacers and increase the spacing between adjacent graphene sheets preventing the irreversible aggregation. But its catalytic activity does not decline significantly. Its mass activity, shown by the MOR peak current, normalized on the basis of Pt loading, was also researched. Interestingly, as can be seen in Fig. 6b, in spite of the 9 % lower Pt active surface area for the G-P-G catalyst, it exhibits a mass activity of 462.8 $A \cdot g^{-1}$ Pt at 0.86 V for methanol electrooxidation (vs. RHE), which is 1.27 times higher than that of Pt/graphene, 363.1 $A \cdot g^{-1}$. Taking into account both effects, the specific activity of the G-P-G catalyst for MOR reaches 0.63 $mA \cdot cm^{-2}$ at 0.86 V, which is also higher than Pt/graphene, 0.45 $mA \cdot cm^{-2}$. Hu et al[41] had reported a large amount of the oxygen-containing groups are present on the surface of graphene, as compared to other carbon materials. It has been known that functional groups, such as -OH, can assist methanol electrooxidation by supplying -OH groups to the intermediates species (for example CO_{ad}), and are responsible for improving the electrocatalytic characteristics. Pt NPs exist between the two adjacent graphene sheets in our synthesized sandwich-structured G-P-G catalyst, hence providing much more oxygen-containing groups than Pt/graphene. Therefore, the G-P-G catalyst has greater catalytic activity than the Pt/graphene catalyst. To further evaluate the activity of the G-P-G catalyst toward the methanol electrooxidation, the commercial Pt/C (E-TEK) was investigated for comparison. As seen from Fig. S6a, It is found that the ESA value of commercial Pt/C (42.3 $m^2 \cdot g^{-1}$) is much lower than that of G-P-G hybrid catalyst. Moreover, Fig. S6b shows the forward peak current density of Pt/C is 305.6 $A \cdot g^{-1}$ Pt at 0.86 V, demonstrating methanol electrooxidation activity of G-P-G catalyst is 1.5 times higher than that of commercial Pt/C. Therefore, the electrocatalytic performance of G-P-G hybrid catalyst can be considered superior to that of Pt/graphene and commercial Pt/C.

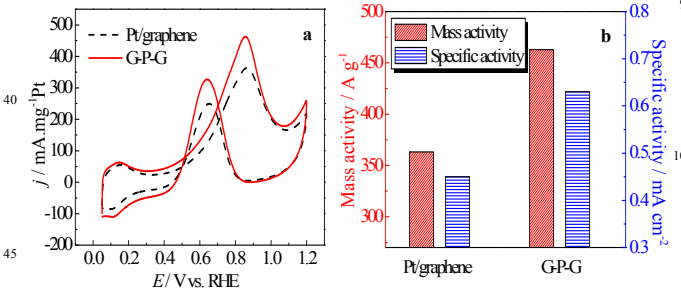

Fig. 6 CV of Pt/graphene and G-P-G catalysts in a solution of 0.5 mol L^{-1} H_2SO_4 containing 0.5 mol L^{-1} CH_3OH. Scanning rate: 50 mV s^{-1}; test temperature: 25 °C (a). Mass activity (MA) and specific activity (SA) at 0.86 V (vs. RHE) for Pt/graphene and G-P-G catalysts (b).

The long-time stability behaviors of Pt/graphene and G-P-G catalysts are investigated by the accelerated potential cycling test (APCT) within the potential range of 0.6 to 1.2 V (vs. RHE). CV before and after APCT are shown in Fig. 7. The ESA of different catalysts with cycle number during the APCT are shown in Fig. 7c, and the normalized ESA are presented in Fig. 7d. It is particularly informative that Pt/graphene has a sharp decline at 1000 cycles and lost nearly 70% of its activity, compared with only 50% for G-P-G catalyst. It demonstrates that G-P-G catalyst possesses 1.7 times as high stability as that of Pt/grapheme. This result indicates that the sandwich-like structure is actually beneficial to the stable property of catalyst. It has been reported graphitic carbon (sp^2-hybridized carbon) on the support, which act as anchoring centers for Pt, can strengthen metal-support interaction and improve the stability.[42] In our prepared sandwich-structured G-P-G catalyst, Pt NPs are anchored between the two adjacent graphene sheets, substantially enhancing metal-support interaction, so the stability has considerably enhanced. Meanwhile, Li and her co-workers[43] reported that the presence of graphene is important in enhancing the durability. Their research suggests that the graphene sheets, with their 2D nature, can possibly act as a "mesh bag" to prevent the Pt species from leaking into the electrolyte. Pt NPs are "wrapped" between the two adjacent graphene sheets for sandwich-structured G-P-G catalyst, so the leaking of Pt species into the electrolyte becomes much more difficult. This may be the reason for the improved stability.

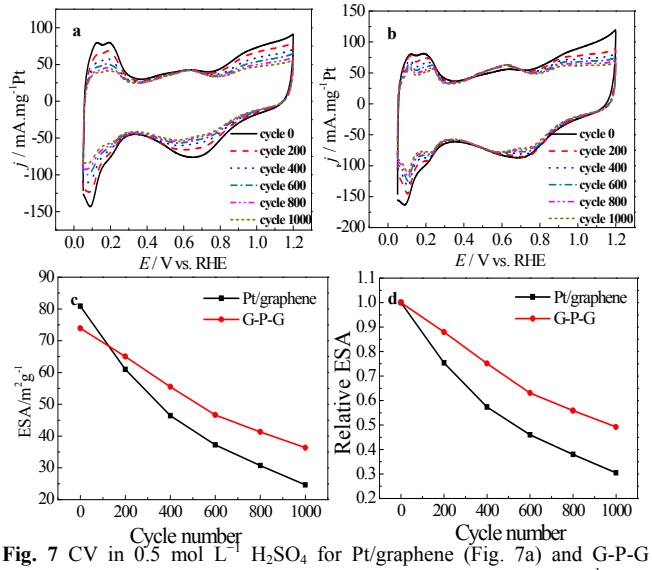

Fig. 7 CV in 0.5 mol L^{-1} H_2SO_4 for Pt/graphene (Fig. 7a) and G-P-G catalysts (Fig. 7b) during the APCT. Scanning rate: 50 mV s^{-1}; test temperature: 25 °C. ESA of Pt/graphene and G-P-G catalysts (Fig. 7c). Relationship of ESA and cycle numbers of Pt/graphene and G-P-G catalysts (Fig. 7d).

The electrocatalytic stabilities of the G-P-G and Pt/graphene catalyst in a solution containing 0.5 mol L^{-1} CH_3OH and 0.5 mol L^{-1} H_2SO_4 have also been compared by using chronoamperometry, as shown in Fig. 8. For both Pt/graphene and G-P-G catalyst, the

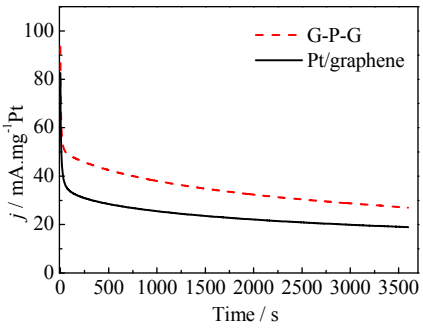

Fig. 8 Chronoamperometric curves for Pt/graphene and G-P-G catalyst in a solution of 0.5 mol L^{-1} H_2SO_4 containing 0.5 mol L^{-1} CH_3OH at a fixed potential of 0.6 V vs. RHE.

potentiostatic current decreases rapidly at the initial stage, which might be due to the formation of intermediate species, such as CO_{ads} and CHO_{ads} etc., during the methanol electrooxidation reaction. It appears that the current density of the G-P-G is higher than that of Pt/graphene catalyst during the whole testing time indicating that the G-P-G hybrid catalyst possesses a higher catalytic stability towards methanol electrooxidation.

To further elucidate the effect of novel sandwich-like structure on the durability enhancement observed, sandwich-structured graphene-Pt/TiO_2-graphene (G-Pt/TiO_2-G) catalyst was synthesized with similar preparation method to G-P-G catalyst. Pt NPs were deposited on the support (graphene + TiO_2) through the MAPP. Then with the introduction of graphene into the mixture, the G-Pt/TiO_2-G hybrid catalyst can be obtained. APCT was carried out to test the durability of the Pt/graphene-TiO_2 and G-Pt/TiO_2-G catalysts. CV before and after APCT are shown in Fig. S7 and the normalized ESA are presented in Fig. 9. It can be found that the ESA of two catalysts decline almost the same during the APCT and both lost 55% at 1000 cycles. The stability of sandwich-structured G-Pt/TiO_2-G is not higher than Pt/graphene-TiO_2 catalyst. Fig. 10 reveals the structure of the two catalysts. The mean size of TiO_2 we used is 20 nm, much larger than that of Pt NPs. When the graphene was introduced into the Pt/graphene-TiO_2 catalyst, graphene will just override the TiO_2 surface, but cannot cover the surface of Pt NPs. Ultimately, G-Pt/TiO_2-G hybrid catalyst was obtained instead of sandwich-structured G-P-G catalyst. Pt NPs will present in the void space between the two adjacent graphene sheets. Pt NPs cannot be anchored by the sandwich-like structured graphene, thus failing to enhance the stability of the catalyst. The above results prove the sandwich-like structure is necessary for the durability enhancement in the negative.

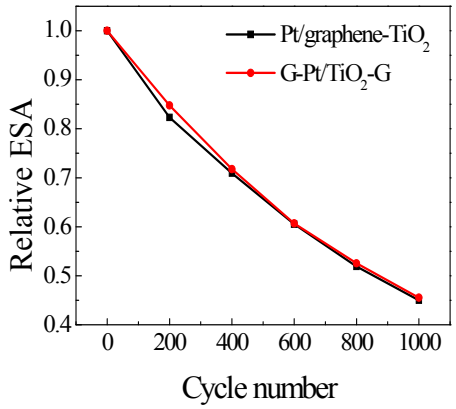

Fig. 9 Relationship of ESA and cycle numbers of Pt/graphene-TiO_2 and G-Pt/TiO_2-G catalysts during the APCT.

It can be observed the novel sandwich-like structure is the key factor to improve the stability. The effect of amount of composited graphene on the stability of G-P-G catalyst has been also investigated. Pt/graphene catalyst was synthesized through MAPP, then with the introduction of different amount of GO into mixture, the desired various G-P-G catalysts can be obtained. Three samples with different amount of introduced GO, namely 30%, 50% and 80%, were prepared, and denoted as G-P-G_{30}, G-P-G_{50} and G-P-G_{80}, respectively. CV before and after APCT are present

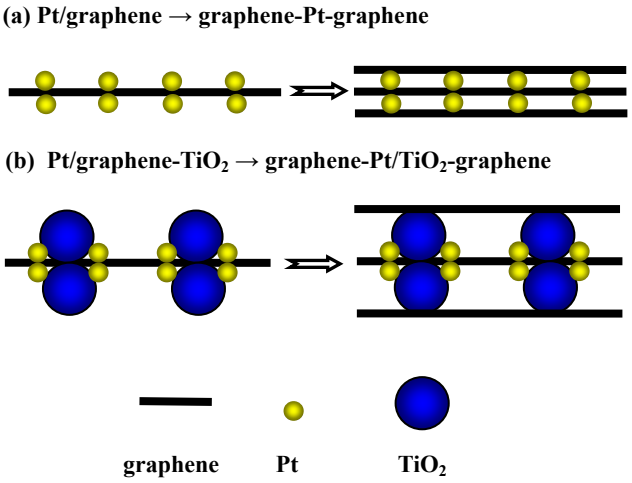

Fig. 10 Structural schematic diagram of G-P-G (a) and G-Pt/TiO_2-G (b) catalysts.

in Fig. S8. The ESA and relative ESA of various G-P-G catalysts with cycle number during the APCT are shown in Fig. 11. As shown in Fig. 11a, the original ESA of the catalysts decrease with the increase of introduced GO amount. That is, the more GO is introduced into the catalyst, the more Pt particle active sites are covered by the sandwich-like structure. However, it can also be distinctly seen that the stability of the catalyst increases with the increase of introduced GO amount. That is probably because Pt NPs are better anchored by the sandwich-like structure with more GO introduced. Taking into account both activity and stability of various G-P-G catalysts, G-P-G_{50} show the optimized electrocatalytic performance.

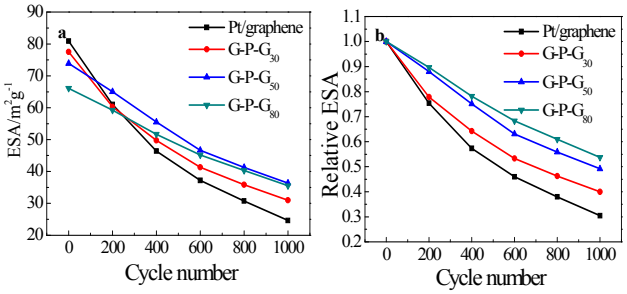

Fig. 11 ESA of Pt/graphene, G-P-G_{30}, G-P-G_{50} and G-P-G_{80} catalysts (a). Relationship of ESA and cycle numbers of various G-P-G catalysts (b).

4. Conclusions

A convenient approach has been developed for the preparation of graphene-Pt-graphene catalyst with a novel sandwich-like structure. The experimental results indicate that the G-P-G exhibits 1.27 times higher activity for methanol electrooxidation than that of Pt/graphene catalyst. Importantly, the G-P-G catalyst possesses 1.7 times as high stability as that of Pt/graphene. The significantly enhanced stability for G-P-G catalyst, in comparison to Pt/graphene, is attributed to the unique sandwich-like structure. Specially, Pt NPs are anchored between the two adjacent graphene sheets, substantially enhancing metal-support interaction and graphene could act as a "mesh bag" to prevent the Pt species from leaking into the electrolyte, so the stability has considerably enhanced. The effect of composited graphene amount in the hybrid

has also been systematically studied. The stability of the catalyst increases with the increasing of introduced GO amount and the G-P-G_{50} show the optimized electrocatalytic performance. This unique catalyst design approach is believed to be a viable, rapid strategy to fabricate high-performance, stable fuel cell electrocatalysts.

Acknowledgment

We acknowledge the National Natural Science Foundation of China (Grant No. 21273058), China postdoctoral science foundation (Grant No.2012M520731 and 2014T70350), Heilongjiang postdoctoral financial assistance (LBH-Z12089) for their financial support.

References

1. M. Z. Jacobson, W. G. Colella and D. M. Golden, *Science*, 2005, 308, 1901-1905.
2. U. Eberle, B. Müller and R. von Helmolt, *Energy Environ. Sci.*, 2012, 5, 8780.
3. S. Guo, S. Zhang and S. Sun, *Angew. Chem. Int. Ed.*, 2013, 52, 8526-8544.
4. R. Borup, J. Meyers, B. Pivovar, Y. S. Kim, R. Mukundan, N. Garland, D. Myers, M. Wilson, F. Garzon, D. Wood, P. Zelenay, K. More, K. Stroh, T. Zawodzinski, J. Boncella, J. E. McGrath, M. Inaba, K. Miyatake, M. Hori, K. Ota, Z. Ogumi, S. Miyata, A. Nishikata, Z. Siroma, Y. Uchimoto, K. Yasuda, K.-i. Kimijima and N. Iwashita, *Chem. Rev.*, 2007, 107, 3904-3951.
5. F. A. de Bruijn, V. A. T. Dam and G. J. M. Janssen, *Fuel Cells*, 2008, 8, 3-22.
6. D. V. Esposito and J. G. Chen, *Energy Environ. Sci.*, 2011, 4, 3900.
7. M. K. Debe, *Nature*, 2012, 486, 43-51.
8. Y. Wang, K. S. Chen, J. Mishler, S. C. Cho and X. C. Adroher, *Appl. Energy*, 2011, 88, 981-1007.
9. T. Matsumoto, T. Komatsu, K. Arai, T. Yamazaki, M. Kijima, H. Shimizu, Y. Takasawa and J. Nakamura, *Chem. Commun.*, 2004, 7, 840-841.
10. Y. Choi, M. Gu, J. Park, H.-K. Song and B.-S. Kim, *Adv. Energy Mater.*, 2012, 2, 1510-1518.
11. D. Wang, H. L. Xin, H. Wang, Y. Yu, E. Rus, D. A. Muller, F. J. DiSalvo and H. D. Abruña, *Chem. Mater.*, 2012, 24, 2274-2281.
12. J. Wu, X. Z. Yuan, J. J. Martin, H. Wang, J. Zhang, J. Shen, S. Wu and W. Merida, *J. Power Sources*, 2008, 184, 104-119.
13. Y.-J. Wang, D. P. Wilkinson and J. Zhang, *Chem. Rev.*, 2011, 111, 7625-7651.
14. M. Roca-Ayats, G. García, M. Peña and M. Martínez-Huerta, *J. Mater. Chem. A*, 2014, 2, 18786-18790.
15. M. Kang, Y.-S. Bae and C.-H. Lee, *Carbon*, 2005, 43, 1512-1516.
16. D. Bom, R. Andrews, D. Jacques, J. Anthony, B. Chen, M. S. Meier and J. P. Selegue, *Nano Lett.*, 2002, 2, 615-619.
17. C. Hu, H. Cheng, Y. Zhao, Y. Hu, Y. Liu, L. Dai and L. Qu, *Adv. Mater.*, 2012, 24, 5493-5498.
18. W. Zhang, J. Chen, G. F. Swiegers, Z. F. Ma and G. G. Wallace, *Nanoscale*, 2010, 2, 282-286.
19. Y. Zhang, L. Jiang, H. Li, L. Fan, W. Hu, C. Wang, Y. Li and S. Yang, *Chemistry*, 2011, 17, 4921-4926.
20. L. Zhao, Z.-B. Wang, X.-L. Sui and G.-P. Yin, *J. Power Sources*, 2014, 245, 637-643.
21. E. S. Steigerwalt, G. A. Deluga, D. E. Cliffel and C. M. Lukehart, *J. Phys. Chem. B*, 2001, 105, 8097-8101.
22. H. Chang, S. H. Joo and C. Pak, *J. Mater. Chem.*, 2007, 17, 3078.
23. K. S. Novoselov, A. K. Geim, S. V. Morozov, D. Jiang, M. I. Katsnelson, I. V. Grigorieva, S. V. Dubonos and A. A. Firsov, *Nature*, 2005, 438, 197-200.
24. S. Stankovich, D. A. Dikin, G. H. B. Dommett, K. M. Kohlhaas, E. J. Zimney, E. A. Stach, R. D. Piner, S. T. Nguyen and R. S. Ruoff, *Nature*, 2006, 442, 282-286.
25. Y. Zhu, D. K. James and J. M. Tour, *Adv. Mater.*, 2012, 24, 4924-4955.
26. A. K. Geim and K. S. Novoselov, *Nature Mater.*, 2007, 6, 183-191.
27. B. Y. Xia, B. Wang, H. B. Wu, Z. Liu, X. Wang and X. W. Lou, *J. Mater. Chem.*, 2012, 22, 16499.
28. X. Wang, X. Li, D. Liu, S. Song and H. Zhang, *Chem. Commun.*, 2012, 48, 2885-2887.
29. Y. Li, L. Tang and J. Li, *Electrochem. Commun.*, 2009, 11, 846-849.
30. Y. Li, W. Gao, L. Ci, C. Wang and P. M. Ajayan, *Carbon*, 2010, 48, 1124-1130.
31. C. Zhu, P. Wang, L. Wang, L. Han and S. Dong, *Nanoscale*, 2011, 3, 4376-4382.
32. R. Kou, Y. Shao, D. Mei, Z. Nie, D. Wang, C. Wang, V. V. Viswanathan, S. Park, I. A. Aksay, Y. Lin, Y. Wang and J. Liu, *J. Am. Chem. Soc.*, 2011, 133, 2541-2547.
33. T. Sun, Z. Zhang, J. Xiao, C. Chen, F. Xiao, S. Wang and Y. Liu, *Sci. Rep.*, 2013, 3.
34. B. Y. Xia, H. B. Wu, J. S. Chen, Z. Wang, X. Wang and X. W. Lou, *Phys. Chem. Chem. Phys.*, 2012, 14, 473-476.
35. D. He, K. Cheng, T. Peng, M. Pan and S. Mu, *J. Mater. Chem. A*, 2013, 1, 2126.
36. Y. Shao, J. Wang, M. Engelhard, C. Wang and Y. Lin, *J. Mater. Chem.*, 2010, 20, 743-748.
37. Z.-Z. Jiang, Z.-B. Wang, Y.-Y. Chu, D.-M. Gu and G.-P. Yin, *Energy Environ. Sci.*, 2011, 4, 728.
38. Y. Xing, *J. Phys. Chem. B*, 2004, 108, 19255-19259.
39. D. Luo, G. Zhang, J. Liu and X. Sun, *J. Phys. Chem. C*, 2011, 115, 11327-11335.
40. H.-L. Guo, X.-F. Wang, Q.-Y. Qian, F.-B. Wang and X.-H. Xia, *Acs Nano*, 2009, 3, 2653-2659.
41. Y. Hu, P. Wu, Y. Yin, H. Zhang and C. Cai, *Appl. Catal. B: environ.*, 2012, 111–112, 208-217.
42. S. Sharma and B. G. Pollet, *J. Power Sources*, 2012, 208, 96-119.
43. Y. Li, Y. Li, E. Zhu, T. McLouth, C.-Y. Chiu, X. Huang and Y. Huang, *J. Am. Chem. Soc.*, 2012, 134, 12326-12329.